Journal of Solid State Chemistry 183 (2010) 1108–1113

Contents lists available at ScienceDirect

Journal of Solid State Chemistry

journal homepage: www.elsevier.com/locate/jssc

Synthesis and characterizations of two anhydrous metal borophosphates: $M_2^{III}BP_3O_{12}$ (M=Fe, In)

Wei-Long Zhang [a,b], Chen-Sheng Lin [a], Lei Geng [a,b], Ye-Yu Li [a,b], Hao Zhang [a], Zhang-Zhen He [a], Wen-Dan Cheng [a,*]

[a] State Key Laboratory of Structural Chemistry, Fujian Institute of Research on the Structure of Matter, Chinese Academy of Sciences, Fuzhou 350002, PR China
[b] Graduate School of the Chinese Academy of Sciences, Beijing 100039, PR China

ARTICLE INFO

Article history:
Received 7 November 2009
Received in revised form
10 March 2010
Accepted 11 March 2010
Available online 19 March 2010

Keywords:
Borophosphates
Solid-state syntheses
3D architecture
Magnetic materials
Band structure

ABSTRACT

Two members of $M_2^{III}BP_3O_{12}$ borophosphates, namely $Fe_2BP_3O_{12}$ and $In_2BP_3O_{12}$, were synthesized by the solid-state method and characterized by the X-ray single crystal diffraction, the powder diffraction and the electron microscopy. They both crystallize in the hexagonal system, space group $P6(3)/m$ (no. 176) and feature 3D architectures, build up of the M_2O_9 units and $B(PO_4)_3$ groups via sharing the corners; however, they are not isomorphic for the different crystallographically distinct atomic positions. Optical property measurements of both compounds and magnetic susceptibility measurements of $Fe_2BP_3O_{12}$ also have been performed. Moreover, in order to gain further insights into the relationship between physical properties and band structure of the $M_2^{III}BP_3O_{12}$ borophosphates, theoretical calculations based on density functional theory (DFT) were performed using the total-energy code CASTEP.

1. Introduction

Borophosphates have been a topic of interest due to their rich structural chemistry and potential applications in sorption and separation, heterogeneous catalysis, photonic technologies, ion exchange, and so on [1–3]. It is known that borates and phosphates exhibit complex structures and tend to form the polynuclear anionic units [4–6]. In general, the B atoms reveal two kinds of coordination modes, either triangular or tetrahedral. The BO_3 and BO_4 groups favor condensation via common corners to form polynuclear anionic units including isolated clusters, infinite chains, sheets, and frameworks; however the PO_4 groups favor condensation via common corners to form different oligomeric units such as P_2O_7, P_3O_{10}, P_4O_{13}, P_6O_{18}, and so on. Considering the excellent properties of borates and phosphates and the diversity structures in the linkage of borate and phosphate, hence, in the search for new functional materials, attention has been partly switched to borophosphates.

So far, a large number of borophosphates containing complex anionic structures extending from isolated species, oligomers, rings, and chains to layers and frameworks have been synthesized under solid-state reactions, supercritical hydrothermal or solvothermal conditions [7–10]. Most of the metal borophosphates were synthesized under hydrothermal conditions [11–15]. Anhydrous phases are rare by high temperature solid reaction, which might have better chemical and thermal stability than the hydrated phase ones to ensure the feasibility of the industrial applications [16–18]. The crystal chemistry of these compounds with anion-group structures mainly built from PO_4 tetrahedra, BO_4 tetrahedra, and planar BO_3 groups, which usually accompany with intriguing magnetism, optics, and so on. As part of this, a series of metal borophosphates with the general formula: $M_2^{III}BP_3O_{12}$ (M=Cr, V) [19,20] have been reported recently. It was mentioned in the literature that Cr_2 BP_3O_{12} crystallizes in hexagonal space group $P3$, which was refined by power diffraction. Compound $V_2BP_3O_{12}$ was structurally characterized by single crystal X-ray diffraction analysis with the space group $P6_3/mc$. In order to enrich this family of $M_2^{III}BP_3O_{12}$ compounds and better understand their structures and characterizations, we will investigate metal borophosphates of ternary systems including Fe, or In. The single crystals of $M_2^{III}BP_3O_{12}$ (M=Fe, In) are selected from the solidified flux dealing with the hot water. Although the compound $Fe_2BP_3O_{12}$ has been reported before [21], its crystal structure has not been characterized in detail. So far, we will report the synthesis of single crystal of $M_2^{III}BP_3O_{12}$ (M=Fe, In) by solid-state reaction and their structural features. Moreover, in order to understand the chemical bonding properties and electronic origins of physical properties for $M_2^{III}BP_3O_{12}$ compounds, we carry out the calculations of crystal energy band

* Corresponding author. Fax: +86 591 83714946.
E-mail addresses: cwd@fjirsm.ac.cn, cwd@ms.fjirsm.ac.cn (W.-D. Cheng).

0022-4596/$ - see front matter © 2010 Elsevier Inc. All rights reserved.
doi:10.1016/j.jssc.2010.03.020

structures, density of states (DOS), and optical response functions of the two title compounds with the density functional theory (DFT) method.

2. Experimental

2.1. Single crystal preparations of compounds $Fe_2BP_3O_{12}$ and $In_2BP_3O_{12}$

Single crystals of $M_2^{III}BP_3O_{12}$ (M=Fe, In) were initially prepared by reactions of a mixture of Cs_2CO_3 (99.9%, Shanghai Chemical Company), H_3BO_3 (Analytical Grade, Shanghai Chemical Company) and $NH_4H_2PO_4$ (Analytical Grade, Shanghai Chemical Company) and M_2O_3 (M=Fe, or In) in a molar ratio corresponding to Cs:M:B:P=2:1:20:12. The addition of Cs_2CO_3 acts as the flux and helps the crystallization of $M_2^{III}BP_3O_{12}$. The mixture was ground in an agate mortar, and then introduced into a platinum crucible. The crucible was heated at 573 K for one day, then heated for two days at 1123 K and cooled down to 923 K at a rate of 3 K/h and finally quenched to room temperature. Some transparent prism-shape crystals were selected carefully from a sintered product with the hot water. After structural analyses, the mono-phase products of $M_2^{III}BP_3O_{12}$ (M=Fe, In) were obtained quantitatively by reacting a mixture of M_2O_3, H_3BO_3, and $NH_4H_2PO_4$ in a molar ratio of 1:1:3 at 1153 K.

2.2. Spectral measurements

X-ray powder diffraction (XRD) pattern was collected on a XPERT-MPD θ–2θ diffractometer to check if the powder sample used for spectral measurement is a single phase. Fig. S1 (in Supplemental Data) gives the powder X-ray diffraction patterns of the two compounds and comparisons with that simulated by the program Visualizer Software using the crystallographic data, confirming the monophasic nature of the prepared samples. IR spectra were recorded on a Magna 750 FT-IR spectrometer photometer as a KBr pellet in the 4000–400 cm^{-1} range. The UV absorption spectra were recorded on a PE Lambda 900 UV–vis spectrophotometer in the wavelength range 200–1800 nm. The absorption spectra were determined by the diffuse-reflectance technique [22]. The absorption spectrum was calculated from reflectance spectrum using the Kubelka–Munk function: $\alpha/S=(1-R)^2/2R$ [23], where α is the absorption coefficient, S is the scattering coefficient. The minima in the second derivative curves of the Kubelka–Munk function is taken as the position of the absorption band.

2.3. Crystal structure determinations

Both single crystals of the two title compounds were selected for indexing, and intensity data collection on SCXmini at the temperature of 293 K and absorption corrections by the multi-scan method were applied for all of them. Lorentz and polarization corrections were applied to the data. Both the structures were solved by direct method and then refined on F2 by full-matrix least-squares method, and performed in the Shelxl/PC programs [24]. All atoms in $Fe_2BP_3O_{12}$ and $In_2BP_3O_{12}$ were refined with anisotropic thermal parameters. None of atoms is disordered and each atomic site is fully occupied according to site occupancy refinements. The final refined solutions obtained were checked with the ADDSYM algorithm in the programme PLATON [25], and no higher symmetry was found. Crystallographic data and structural refinements for the three compounds are summarized in Table 1. The atomic coordinates and selected important bond lengths are listed in Tables 2 and 3, respectively. Crystallographic data in CIF format for $Fe_2BP_3O_{12}$ and $In_2BP_3O_{12}$ have been given as Supporting Materials. These data can also be obtained from the Fachinformationszentrum Karlsruhe, 76344 Eggenstein-Leopoldshafen, Germany (fax: +49 7247 808 666; e-mail: crysdata@fiz-karlsruhe.de) on quoting the depository numbers CSD 420638 and 420643.

Table 1
Crystal data and structural refinements for $Fe_2BP_3O_{12}$ and $In_2BP_3O_{12}$.

	Compound **1**	Compound **2**
Formula	$Fe_2BP_3O_{12}$	$In_2BP_3O_{12}$
Fw	407.42	525.36
Space group	$P6(3)/m$ (no. 176)	$P6(3)/m$ (no. 176)
a (Å)	8.0306(9)	8.1698(6)
b (Å)	8.0306(9)	8.1698(6)
c (Å)	7.4089(13)	7.7375(11)
α (deg)	90	90
β (deg)	90	90
γ (deg)	120	120
V (Å^3)	413.79(10)	447.25(8)
Z	2	2
D_{calcd} (g cm^{-3})	3.270	3.901
μ (mm^{-1})	4.160	5.763
GOF on F^2	1.136	1.035
R_1, wR_2 [$I>2\sigma(I)$][a]	0.0268, 0.0528	0.0134, 0.0329
R_1, wR_2 (all data)	0.0307, 0.0543	0.0135, 0.0330

[a] $R_1=\sum||F_o|-|F_c||/\sum|F_o|$, $wR_2=\{\sum w[(F_o)^2-(F_c)^2]^2/\sum w[(F_o)^2]^2\}^{1/2}$.

Table 2
Atomic coordinates ($\times 10^4$) and displacement parameters ($A^2\times 10^3$) for $Fe_2BP_3O_{12}$ and $In_2BP_3O_{12}$.

Atom	x	y	z	$U(_{eq})$[a]
$Fe_2BP_3O_{12}$				
Fe(1)	3333	6667	−481(1)	8(1)
P(1)	450(1)	3604(1)	2500	7(1)
O(1)	−571(4)	1333(4)	2500	11(1)
O(2)	1624(3)	4342(3)	797(2)	12(1)
O(3)	−1263(4)	3951(4)	2500	8(1)
B(1)	0	0	2500	10(1)
$In_2BP_3O_{12}$				
In(1)	3333	6667	−442(1)	7(1)
P(1)	−3506(1)	−417(1)	2500	7(1)
O(1)	−1269(3)	611(3)	2500	10(1)
O(2)	−4201(2)	−1540(2)	866(2)	8(1)
O(3)	−3886(3)	1251(3)	2500	14(1)
B(1)	0	0	2500	10(1)

[a] U_{eq} is defined as one-third of the trace of the orthogonalized U_{ij} tensor.

2.4. Magnetic susceptibility

Variable-temperature (2.0–300 K) magnetic susceptibility measurement on polycrystalline sample of $Fe_2BP_3O_{12}$ was carried out on a Quantum Design MPMS-XL SQUID magnetometer. The raw data were corrected for the susceptibility of the container and the diamagnetic contributions of the sample using Pascal constants.

2.5. Computational details

The crystallographic data of $In_2BP_3O_{12}$ and $Fe_2BP_3O_{12}$ determined by X-ray single crystal diffraction were used for the band structure calculations, no further geometry optimizations were performed in theoretical study. The calculations of band structure were made by the density functional theory (DFT) with the Perdew–Burke–Ernzerh of generalized gradient approximation

Table 3
Selected bond lengths (Å) for $Fe_2BP_3O_{12}$ and $In_2BP_3O_{12}$.

$Fe_2BP_3O_{12}$					
Fe(1)–O(2)♯#1	1.9243(19)	Fe(1)–O(2)	1.9243(19)	Fe(1)–O(2)♯2	1.9243(19)
Fe(1)–O(3)♯3	2.1029(18)	Fe(1)–O(3)♯4	2.1029(18)	Fe(1)–O(3)♯5	2.1029(18)
P(1)–O(2)♯7	1.5079(18)	P(1)–O(2)	1.5079(18)	P(1)–O(3)	1.535(3)
P(1)–O(1)	1.582(3)	B(1)–O(1)♯9	1.359(3)	B(1)–O(1)♯10	1.359(3)
B(1)–O(1)	1.359(3)				
$In_2BP_3O_{12}$					
In(1)–O(2)♯1	2.0679(17)	In(1)–O(2)♯2	2.0679(17)	In(1)–O(2)♯3	2.0679(17)
In(1)–O(3)♯4	2.2060(16)	In(1)–O(3)♯5	2.2060(17)	In(1)–O(3)♯6	2.2060(17)
P(1)–O(2)♯117	1.4973(18)	P(1)–O(2)	1.4973(18)	P(1)–O(3)	1.541(2)
P(1)–O(1)	1.585(2)	B(1)–O(1)♯3	1.357(2)	B(1)–O(1)♯10	1.357(2)
B(1)–O(1)	1.357(2)				

Symmetry transformations used to generate equivalent atoms:
For $Fe_2BP_3O_{12}$: ♯1 $-x+y, -x+1, z$; #2 $-y+1, x-y+1, z$; ♯3 $-x, -y+1, -z$; #4 $x-y+1, x+1, z-1/2$; ♯5 $y, -x+y, -z$; ♯6 $-x+y, -x+1, -z-1/2$; ♯7 $x, y, -z+1/2$; ♯8 $x-y, x, z+1/2$; ♯9 $-y, x-y, z$; ♯10 $-x+y, -x, -z+1/2$.
For $In_2BP_3O_{12}$: ♯1 $-y, x-y+1, z$; ♯2 $x+1, y+1, z$; #3 $-x+y, -x, z$; ♯4 $-x, -y+1, -z$; ♯5 $y, -x+y, -z$; #6 $x-y+1, x+1, -z$; ♯7 $x, y, -z-1/2$; ♯8, $-x, -y+1, z+1/2$; ♯9 $x-1, y-1, z$; ♯10 $-y, x-y, z$, #11 $x, y, -z+1/2$.

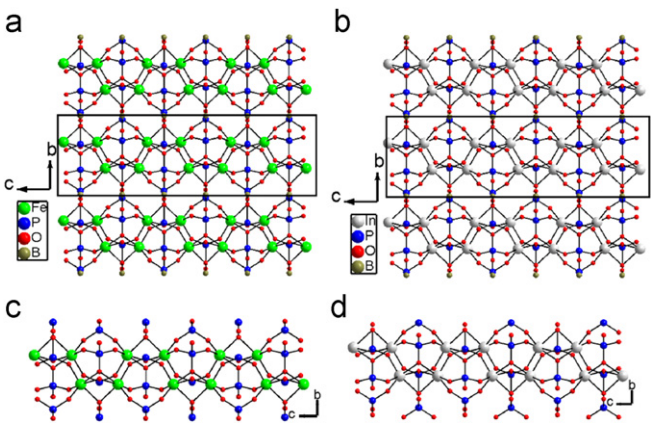

Fig. 1. View the structure of the $Fe_2BP_3O_{12}$ (a) and $In_2BP_3O_{12}$ (b) along *a* axis and the layer of $[Fe_2P_3O_{12}]_n^{3n-}$ (c) and $[In_2P_3O_{12}]_n^{3n-}$ (d) in the *ac* plane. Fe, In, B, P, and O atoms are represented by green, gray, dark yellow, blue, and red, respectively. (For interpretation of the references to color in this figure legend, the reader is referred to the web version of this article.)

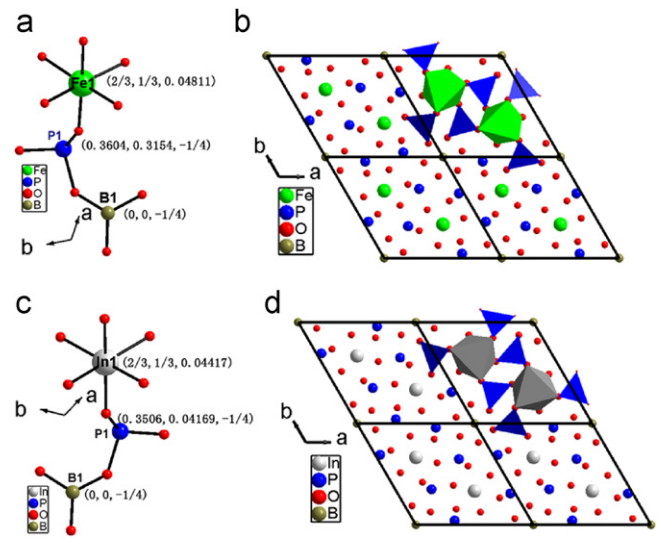

Fig. 2. The selected units of $Fe_2BP_3O_{12}$ (a), and $In_2BP_3O_{12}$ (c), and view the structures of the $Fe_2BP_3O_{12}$ (b), and $In_2BP_3O_{12}$ (d) along *c* axis. FeO_6 octahedra, InO_6 octahedra, and PO_4 tetrahedra are shaded in green, gray, and blue, respectively. B and O atom are represented by dark yellow and red, respectively. (For interpretation of the references to color in this figure legend, the reader is referred to the web version of this article.)

[26] and performed with the CASTEP code [27], which uses a plane wave basis set for the valence electrons and norm-conserving pseudopotential [28] for the core states. The following orbital electrons were treated as valence electrons: In-$4d^{10}5s^25p^1$, Fe-$3d^64s^2$, B-$2s^22p^1$, P-$3s^23p^3$ and O-$2s^22p^4$. Considering the balance of computational cost and precision, we chose the cutoff energy of 500 eV and a $4\times4\times4$ Monkhorst–Pack *k*-point samplings for $In_2BP_3O_{12}$, a cutoff energy of 500 eV and a $4\times4\times3$ Monkhorst–Pack *k*-point sampling for $Fe_2BP_3O_{12}$. Spin polarization was included for the electronic structure calculations of $Fe_2BP_3O_{12}$ and the space group symmetry used for the AF calculation for the iron compound was P1, see Fig. S2 (in Supplemental Data). The other calculating parameters used in the calculations and convergent criteria were set by the default values of the *CASTEP* code.

3. Results and discussions

3.1. Structural descriptions

High-temperature solid-state reactions of Fe_2O_3 (or In_2O_3), H_3BO_3, $NH_4H_2PO_4$ afforded two new quaternary compounds, namely, $M_2^{III}BP_3O_{12}$ (M=Fe, In). X-Ray analysis revealed that the compounds $M_2^{III}BP_3O_{12}$ (M=Fe, In) both crystallize in the hexagonal system, space group $P6(3)/m$ (no. 176) and feature 3D architectures build up of the M_2O_9 units and $B(PO_4)_3$ groups via sharing the corners, but they are not isomorphic for the different atomic positions.

Both $Fe_2BP_3O_{12}$ and $In_2BP_3O_{12}$ feature 3D architectures decorated by M_2O_9 units, BO_3 and PO_4 groups via sharing the corners. The structure of $M_2BP_3O_{12}$ (M=Fe, In) feature complicated 3D networks in which layers of $[M_2P_3O_{12}]_n^{3n-}$ (M=Fe, In) in the ac plane are further interconnected by bridging BO_3 (Fig. 1). When viewing the layer of $[Fe_2P_3O_{12}]_n^{3n-}$ and $[In_2P_3O_{12}]_n^{3n-}$ along the axis of *a*, we will found that the two title compounds are different (see Fig. 2), so it is better to say that two compounds are not isomorphic. There is one crystallographically distinct Fe (In) atom, one B atom, one P atom and three O atoms in the asymmetric unit of $M_2BP_3O_{12}$ (M=Fe, In). From the selected units of $Fe_2BP_3O_{12}$ (Fig. 2(a)), and $In_2BP_3O_{12}$ (Fig. 2(c)), we can find out the differences between the two compounds easily, B atoms in asymmetric units of the two compounds present in the same sit of (0, 0, 0.25), and Fe atoms (1/3, 2/3, 0.48) and In atoms (1/3, 2/3,

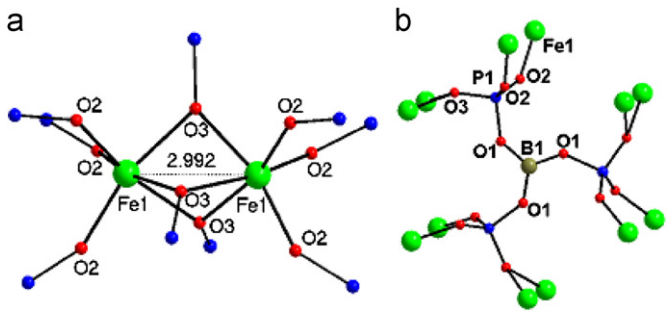

Fig. 3. The coordination of $[Fe1_2O_9]$ dimmer (a), and the coordination of oxygen atoms around $[BP_3O_{12}]^{6-}$ units (b). Fe, B, P, and O atom are represented by green, dark yellow, blue, and red, respectively (For interpretation of the references to color in this figure legend, the reader is referred to the web version of this article.)

0.42) are almost located in the same sit, but P atoms are quit different with (0.45, 0.36, 0.25) and (−0.35, −0.42, 0.25) in asymmetric units of $Fe_2BP_3O_{12}$ and $In_2BP_3O_{12}$, respectively.

Though the two compounds are not isomorphic for the different positions of crystallographically distinct atoms, they have the same inorganic connectivity terms. We take the compound of $Fe_2BP_3O_{12}$ as a representative, the projection of this structure concerns about a dimer $[Fe_2O_9]$ forming by the adjacent two face-sharing $[Fe1O_6]$ octahedra (see Fig. 3a). Fe atoms are octahedrally coordinated by six oxygen atoms with the Fe–O distances ranging from 1.9243(19) to 2.1029(18) Å, which are comparable to other iron borophosphates [29,30]. Each B atom is trigonal coordinated by three oxygen atoms (Fig. 3b), forming nearly ideal BO_3 triangle with three equal B–O bond lengths of 1.359(3) Å, while each P atom is tetrahedral coordinated by four oxygen atoms in a tetrahedral geometry with three types of P–O distances (1.508(18), 1.535(6), and 1.582(2) Å), these B–O and P–O bond distances are also comparable to other metal borophosphates [31]. The 3D architecture can also be viewed as each BO_3 are connected to three PO_4 via corner-sharing O1 atoms to form a zero-dimensional (0D) anionic unit of $[BP_3O_{12}]^{6-}$, Then adjacent $[BP_3O_{12}]^{6-}$ units are further connected by the FeO_6 octahedra, forming the 3D framework of $Fe_2BP_3O_{12}$. For compound $In_2BP_3O_{12}$ (Table 3), the In–O bond distances are ranging from 2.0679(17) to 2.2060(17) Å, the B atoms are also forming nearly ideal BO_3 triangle with three equal B–O bond lengths of 1.357(2) Å, the P–O bond distances are ranging from 1.4973(18) to 1.585(2) Å, which are comparable to $Fe_2BP_3O_{12}$ discussed above.

Results of bond-valence calculations indicate that Fe, In, B, and P atoms are reasonable oxidation states with +3, +3, +3, and +5, respectively, for compounds $Fe_2BP_3O_{12}$ and $In_2BP_3O_{12}$. The calculated total bond valences are 3.13, 3.09, and 4.86 for Fe1, B1, and P1 in compound $Fe_2BP_3O_{12}$, 3.23, 3.10, and 4.91 for In1, B1, and P1 in compound $In_2BP_3O_{12}$, respectively.

3.2. Optical properties of $In_2^{III}BP_3O_{12}$ and magnetic properties of $Fe_2^{III}BP_3O_{12}$

IR studies indicate that both two compounds are transparent in the range of 4000–1700 cm^{-1} (2.5–5.9 μm). IR spectra of two title compounds display similar features with other metal borophosphates [32], and taking $In_2BP_3O_{12}$ as a representation in the following discussions (Fig. S3a in Supplemental Data). It indicates that the $In_2BP_3O_{12}$ is transparent in the range of 4000–1400 cm^{-1}. Peaks were observed for cobalt compound at: 497, 542, 608, 643, 901, 955, 1106, 1382, and the iron compound has similar peaks (Fig. S3b in Supplemental Data) [16]. Stretching and bending frequencies of B–O and P–O groups are observed up to 1400 cm^{-1}. The bands at 1382 and 1106 cm^{-1} are the asymmetric stretching and symmetric stretching of B–O in BO_3, respectively. The bands at 643, 508, and 497 cm^{-1} are the out-of plane bending of B–O in BO_3. The optical diffuse-reflectance spectra indicate optical band gaps of 5.39 and 3.52 eV for $In_2BP_3O_{12}$ and $Fe_2BP_3O_{12}$ (Fig. 4).

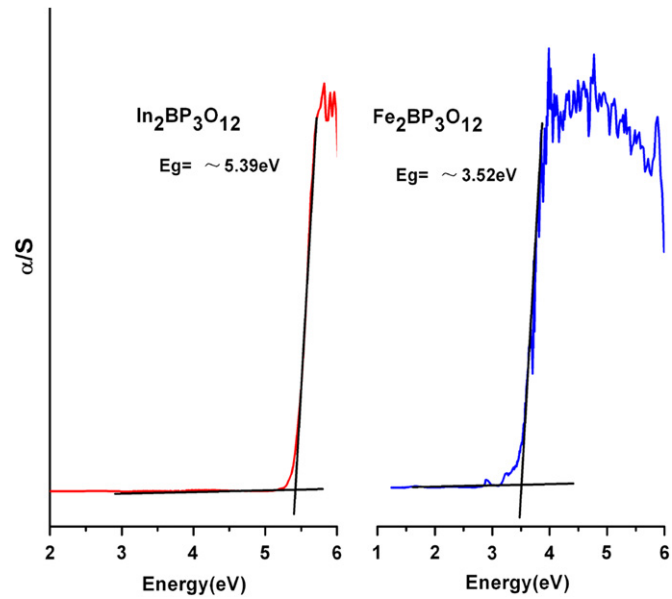

Fig. 4. Optical diffuse reflectance spectra for $In_2BP_3O_{12}$ and $Fe_2BP_3O_{12}$.

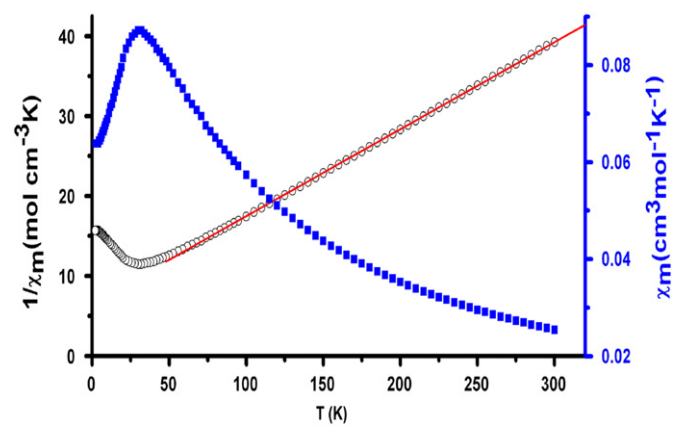

Fig. 5. $1/\chi$ vs T and χ vs T plots for $Fe_2BP_3O_{12}$. The red line represents the linear fit of data according to the Curie–Weiss law. (For interpretation of the references to color in this figure legend, the reader is referred to the web version of this article.)

3.3. Magnetic properties

The dc magnetic properties of $Fe_2BP_3O_{12}$ were measured in the temperature range of 2–300 K at the applied magnetic field of 1000 Oe. Fig. 5 shows the temperature dependences of the magnetic susceptibility for polycrystalline $Fe_2BP_3O_{12}$. A sharp peak is observed at 30.9 K, indicating the onset of antiferromagnetic (AF) ordering. Above 50 K, the susceptibility increases with decreasing temperature, a typical Curie–Weiss behavior is observed, giving the Curie constant $C=9.18(4)$ emu K/mol and Weiss constant $\Theta=-60.39(2)$ K. The effective magnetic moment of Fe^{3+} ions in the system is calculated to be $6.06(1)\mu_B$, which is larger than the value $5.91(6)\mu_B$ obtained by Fe^{3+} ($S=5/2$) ions, indicating that Fe^{3+} ions have a high spin state

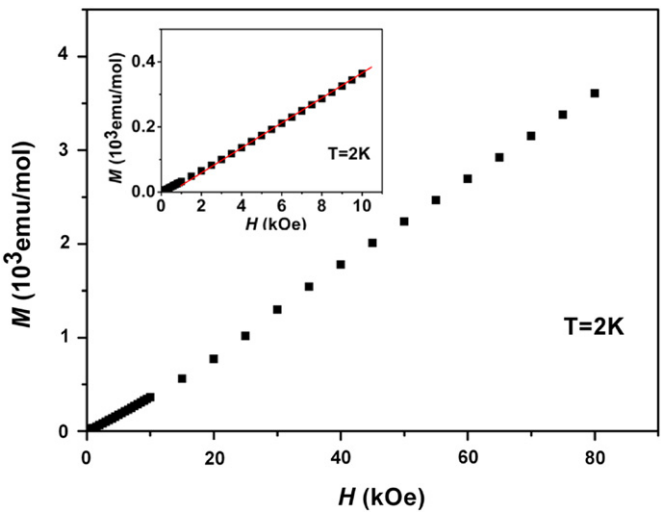

Fig. 6. Magnetization (M) as a function of magnetic field (H) for $Fe_2BP_3O_{12}$.

and a little orbital moment contribution of Fe^{3+} in oxygen octahedral environment. Also, the negative Weiss temperature indicates that considerably stronger antiferromagnetic coupling dominates the exchange between iron atoms. It is expected that the magnetic interaction mainly occurred within and between iron dimmers (Fig. 3a), in which the two magnetic atoms are interconnected via Fe–O–Fe bridges with a Fe⋯Fe separation of 2.9991 Å and Fe–O–Fe angle of 90.67°. Fig. 6 shows magnetization (M) as a function of applied field (H) at $T=2$ K. A linear increase in magnetization is observed for $Fe_2BP_3O_{12}$, agreeing with an AF ordering below 30.9 K, while a slight increase is observed at around $H=1.5$ koe, presumably indicating a field-induced spin-flop transition.

3.3. Band structures and density of states (DOS)

To gain further insights into the relation between electronic structure and optical properties of $M_2^{III}BP_3O_{12}$ compounds, band structure and density of states (DOS) calculations of two title compounds based on density functional theory (DFT) were performed using the total-energy code CASTEP.

The calculated band structures of $In_2BP_3O_{12}$ and $Fe_2BP_3O_{12}$ along high-symmetry points within the first Brillouin zone are plotted in Fig. S4 (in Supplemental Data). It is found that the top of valence bands (VBs) is almost flat, whereas the bottom of conduction bands (CBs) displays some dispersion for the compound $In_2BP_3O_{12}$. The state energies (eV) of the lowest conduction band (L-CB) and the highest valence band (H-VB) at some k points of both compounds are listed in Table S1. For $In_2BP_3O_{12}$, both the top of valence bands (VB) and the bottom of conduction bands (CB) are located at the G point; hence, $In_2BP_3O_{12}$ is a compound with direct band gap. For $Fe_2BP_3O_{12}$, the lowest energy at the CBs (2.81 eV) is located at the F point, whereas the highest energy of VBs at F points is a very close to 0.0 eV; hence, $Fe_2BP_3O_{12}$ has an approximately direct band gap of 2.81 eV, which is much smaller than that of $In_2BP_3O_{12}$. The calculated direct band gaps are 3.75 and 2.81 eV, which are smaller than the experimental results of 5.39 and 3.52 eV for $In_2BP_3O_{12}$ and $Fe_2BP_3O_{12}$, respectively. The discrepancy is due to the limitation of DFT method that generally underestimates the band gap in semiconductors and insulators [32–34].

The bands can be assigned according to the total and partial densities of states (DOS) as plotted in Fig. 7. The regions below the Fermi level (the Fermi level is set at 0 eV) of both compounds are

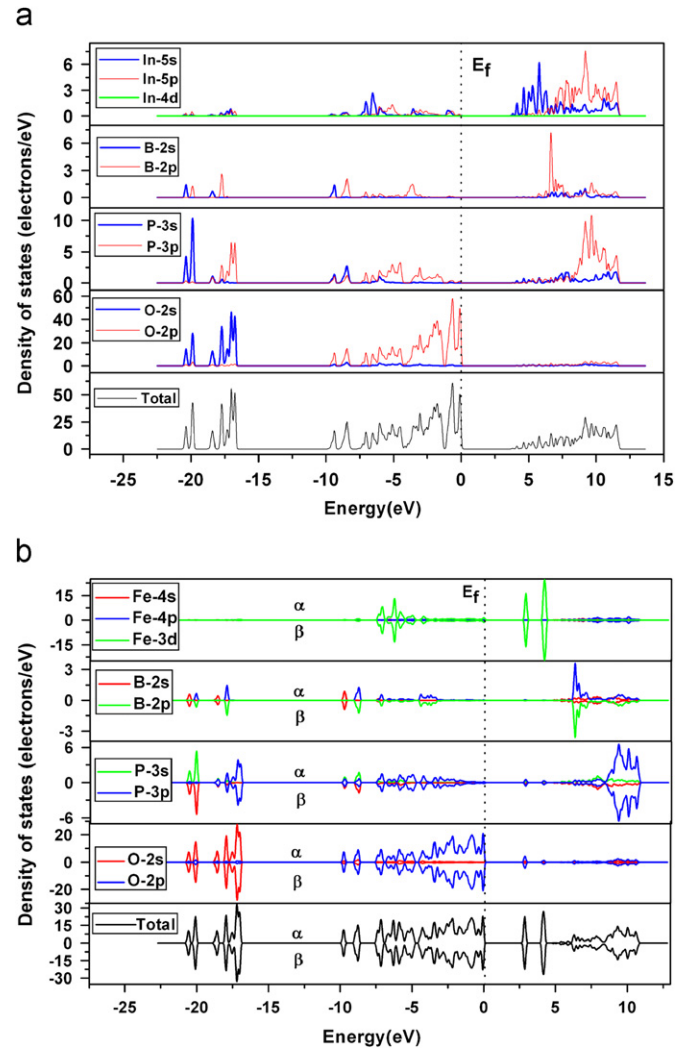

Fig. 7. Total and partial DOS of $In_2BP_3O_{12}$ (a) and $Fe_2BP_3O_{12}$ (b). The Fermi level is set at 0 eV.

quite similar, which can be divided into four regions. The VBs ranging from −21.9 to −15.0 eV are mainly composed of O-2s, and B-2s states mixing with a small amount of the P-3p and O-2p states. The VBs ranging from −15.0 to −7.5 eV are mainly formed B-2s, P-3s and O-2s states are mainly formed by In-5s (Fe-3d) state mixing with a small amount of the B-2s2p, P-3s3p and O-2p states. The VBs ranging from −7.5 to −4.0 eV are mainly formed by O-2p and P-3p states (Fe-3d) state, and Fe-3d (In-5s) filled around −7, The VBs ranging from −4.0 eV to Fermi level (0.0 eV) are mainly contributions from the O-2p states. The bands just above the Fermi level are different for two compounds. For $Fe_2BP_3O_{12}$, the states of empty Fe-3d dominate the CBs ranging from 2.0 to 4.0 eV, whereas the CBs ranging from 5.0 to 15 eV are mainly composed of the states of B-2p, P-3p, and mixing with a small amount of the B-2s and P-3s states. For $In_2BP_3O_{12}$, the CBs above the Fermi level can be divided into three regions, In-5s filled around 5.0 eV, B-2p filled around 6.0 eV, In-5p and P-3p dominate the CBs above 6.0 eV. The calculated populations show that the B–O bonds and P–O bonds are substantial covalence features. From analyses of the curves of the averaged imaginary part (Fig. S5 in Supplemental Data), the observed strongest adsorption peaks are at about 9.52 eV, which can be mainly assigned as the electronic interband transitions from the O-2p to In-5s states and from the O-2p to Fe-3d states for $In_2BP_3O_{12}$ and $Fe_2BP_3O_{12}$, respectively.

4. Conclusion

In summary, two new single crystals of metal borophosphates $M_2^{III}BP_3O_{12}$ (M=Fe, In) have been synthesized by solid-state method and structurally characterized by X-ray single crystal. The two compounds are not isomorphic for the different crystallographically distinct atomic positions but with the same inorganic connectivity terms. The structure of $M_2BP_3O_{12}$ features a complicated 3D network in which layers of $[M_2P_3O_{12}]_n^{3n-}$ in the *ac* plane are further interconnected by bridging BO_3. The projections of these structures are concerning about the dimmer $[M_2O_9]$ forming by the face-sharing of the MO_6 octahedra. The inverse magnetic susceptibility of $Fe_2BP_3O_{12}$ in the range of 50–300 K obeys the Curie–Weiss law with a big negative Weiss constant θ of -60.39 K indicating that considerably stronger antiferromagnetic coupling dominates the exchange between iron atoms. The observed strongest adsorption peaks can be assigned as the electronic transitions from the O-2*p* to In-5*s* states and from the O-2*p* to Fe-3*d* states for $In_2BP_3O_{12}$ and $Fe_2BP_3O_{12}$, respectively, in terms of the evaluations from calculated band structures and density of states.

Acknowledgments

This investigation was based on work supported by the National Natural Science Foundation of China under Project 20773131, the National Basic Research Program of China (no. 2007CB815307) and the Funds of Chinese Academy of Sciences (KJCX2-YHW01, FJIRSM-SZD07001), and Fujian Key Laboratory of Nanomaterials (no. 2006L2005).

Appendix A. Supplementary Data

Supplementary data associated with this article can be found in the online version at doi:10.1016/j.jssc.2010.03.020.

References

[1] S.L. Pan, Y.-C. Wu, P.-Z. Fu, G.-C. Zhang, Z.-H. Li, C.X. Du, C.-T. Chen, Chem. Mater. 15 (2003) 2218.
[2] Z.-H. Li, Z.-S. Lin, Y.-C. Wu, P.Z. Fu, Z.Z. Wang, C.T. Chen, Chem. Mater. 16 (2004) 2906.
[3] G.F. Wang, Y.C. Wu, P.Z. Fu, X.Y. Liang, Z.Y. Xu, C.T. Chen, Chem. Mater. 14 (2002) 2044.
[4] G. Heller, Top. Curr. Chem. 131 (1986) 39.
[5] R.C. Haushalter, L.A. Mundi, Chem. Mater. 4 (1992) 31.
[6] W.L. Zhang, W.D. Cheng, H. Zhang, L. Geng, Y.Y. Li, C.S. Lin, Z.Z. He, Inorg. Chem. 49 (2010) 2550.
[7] R. Kniep, H. Engelhardt, C. Hauf, Chem. Mater. 10 (1998) 2930.
[8] R. Kniep, H.G. Will, I. Boy, C. Röhr, Angew. Chem. 109 (1997) 1052.
[9] H. Ehrenberg, S. Laubach, P.C. Schmidt, R. McSweeney, M. Knapp, K.C. Mishra, J. Solid State Chem. 179 (2006) 968.
[10] R.P. Bontchev, S.C. Sevov, Inorg. Chem. 35 (1996) 6910.
[11] T. Yang, J.-L. Sun, G.-B. Li, L. Eriksson, X.-D. Zou, F.-H. Liao, J.-H. Lin, Chem. Eur. J. 14 (2008) 7212.
[12] W.-T. Yang, J.-Y. Li, Q.-H. Pan, Z. Jin, J.-H. Yu, R.-R. Xu, Chem. Mater. 20 (2008) 4900.
[13] E. Dumas, C. Debiemme-Chouvy, S.C. Sevov, J. Am. Chem. Soc. 124 (2002) 908.
[14] W. Liu, M.-R. Li, H.-H. Chen, X.-X. Yang, J.-T. Zhao, Dalton Trans. (2004) 2847.
[15] P.W. Menezes, S. Hoffmann, Y. Prots, R. Kniep, Z. Anorg. Allg. Chem. 635 (2009) 614.
[16] D. Zhao, W.-D. Cheng, H. Zhang, S.-P. Huang, Z. Xie, W.-L. Zhang, S.-L. Yang, Inorg. Chem. 48 (2009) 6623.
[17] R. Kniep, G. Gozel, B. Eisenmann, C. Röhr, M. Asbrand, M. Kizilyalli, Angew. Chem. Int. Ed. Engl. 33 (1994) 791.
[18] D.-B. Xiong, H.-H. Chen, X.-X. Yang, J.-T. Zhao, J. Solid State Chem. 180 (2007) 233.
[19] J.-X. Mi, J.-T. Zhao, S.-Y. Mao, Y.-X. Huang, H. Engelhardt, R. Kniep, Z. Kristallogr, New Cryst. Struct. 215 (2000) 201.
[20] M. Meisel, M. Paech, L. Wilde, D. Wulff-Molder, Z. Anorg. Allg. Chem. 630 (2004) 983.
[21] H.-H. Chen, M.-H. Ge, X.-X. Yang, J.-X. Mi, J.-T. Zhao, J. Inorg. Mater. 19 (2004) 429.
[22] P. Kubelka, F.Z. Munk, Tech. Phys. 12 (1931) 593.
[23] W.M. Wendlandt, H.G. Hecht, Reflectance Spectroscopy, Interscience, New York, 1966.
[24] G.M. Sheldrick, SHELXTL-97 Program for Refining Crystal Structure, University of Göttingen, Göttingen, Germany, 1997.
[25] A.L. Spek, J. Appl. Cryst. 36 (2003) 7.
[26] J.P. Perdew, K. Burke, M. Ernzerhof, Phys. Rev. Lett. 77 (1996) 3865.
[27] M.D. Segall, P.L.D. Lindan, M.J. Probert, C.J. Pickard, P.J. Hasnip, S.J. Clark, M.C. Payne, J. Phys. Condens. Matter 14 (2002) 2717.
[28] D.R. Hamann, M. Schluter, C. Chiang, Phys. Rev. Lett. 43 (1979) 1494.
[29] T. Yang, G.B. Li, J. Ju, F.H. Liao, M. Xiong, J.H. Lin, J. Solid State Chem. 179 (2006) 2534.
[30] Y.-X. Huang, B. Ewald, W. Schnelle, Yu. Prots', R. Kniep, Inorg. Chem. 45 (2006) 7578.
[31] H.W. Ma, J.K. Liang, L. Wu, G.Y. Liu, G.H. Rao, X.L. Chen, J. Solid State Chem. 177 (2004) 3454.
[32] W.L. Zhang, X.S. Lin, H. Zhang, J.Y. Wang, C.S. Lin, Z.Z. He, W.D. Cheng, Dalton Trans. 39 (2010) 1546.
[33] J. Zhu, W.-D. Cheng, D.-S. Wu, H. Zhang, Y.-J. Gong, H.-N. Tong, D. Zhao, Inorg. Chem. 46 (2007) 208.
[34] C.M.I. Okoye, J. Phys. Condens. Matter 15 (2003) 5945.